NUMERICAL ANALYSIS OF THE BEHAVIOR OF PHOTOCHEMICAL PRODUCTS IN LOCAL FLOWS OVER CENTRAL JAPAN IN SUMMER SEASON -SENSITIVITY OF OZONE CONCENTRATION TO EMISSION SOURCES OVER COASTAL URBAN AREAS-

Toshihiro Kitada[1)]*, and Kiyoshi Okamura[2)]

1) Dept. of Ecological Engineering, Toyohashi University of Technology
Tempaku-cho, Toyohashi, Japan 441-8580
2) Department of Environmental Information, Nagoya Sangyo University
Arai-machi, Owari-asahi, Japan 488-8711
* Corresponding author; E-mail, kitada@earth.eco.tut.ac.jp

Abstract

Air pollution transport over Central Japan was numerically simulated in a typical land and sea breeze situation in summer season. The models used in the calculation were extensions of those described in Kitada et al. (1993) and (1998). Sensitivity of the production of ozone and acidic species to emissions of biogenic non-methane-hydrocarbon (NMHC), and anthropogenic-NMHC and -NOx were focused; the ozone, sulfate, and nitrate are chemically produced in pollutants-rich air mass migrating from coastal big cities to central mountains. Some of the obtained results are as follows: (1) biogenic hydrocarbons could increase daily maximum ozone concentration as much as 20 ppb over the Nohbi and Kanto Plains, and (2) reduction of NOx emission by 20% may result in increase of the ozone concentration by a few percent to almost 20% over the Nohbi Plain, indicating necessity of careful emission control.

Key words : local winds, photochemical smog, ozone, biogenic hydrocarbon, Japan, numerical simulation.

1. INTRODUCTION

The central Japan has characteristic topographical features such as many high mountains and large plains, and is bounded with complex coast lines for Pacific Ocean at the south side and for the Sea of Japan at the north side. Thus various types of local flows develop in this area in summer season. In the daytime flow system pollutants emitted over the huge coastal-urban areas in the plains such as Tokyo, Nagoya, and Osaka likely reach to the mountainous central part in a day, located 150 km from the Pacific Ocean, with producing ozone and others. More than 10 years ago, this phenomenon was extensively studied with observations in the Kanto Plain, i.e. Tokyo area, and the flow system has been named the “extended sea breeze”. However, the subsequent behavior and fate of the ozone and other products are not clear. In this study; 3D three-days-simulations, during 26-28 July, 1995, of transport, chemistry and deposition of various chemical species were performed to see the behavior of ozone etc.

produced in the pollutants clouds discharged from the urban area, particularly Nagoya in the Nohbi Plain, for the calculation domain over the Central Japan, with the size of 550 km x 450 km x 6.5 km for east-west, north-south, and vertical directions, respectively The simulation results showed that the high ozone once produced and transported to mountainous area is returned back into the upper layer with its center around 1000 m high over the coastal area on the subsequent day. These were well compared with the vertical profiles of ozone obtained with aircraft observations over the coastal Nohbi Plain and the Ise Bay; the aircraft observations were performed as the part of environmental assessment on a new international airport to be constructed in the Ise Bay Total ozone produced over the Central Japan was evaluated as well as the amount of deposited acidic pollutants.

2. BACKGROUND OF THE PROBLEM

Medium range transport of air pollutants from highly developed urban area to mountainous rural area has attracted concern of many people in applied meteorology and atmospheric environment in Japan, since it occurs in an interesting combination of several types of local winds such as land and sea breezes, mountain and valley winds, and plain-plateau winds, and the transport repeated in summer season probably causes severe damage for eco-systems in the mountainous area. Kurita et al. (1985) pointed out that the pollutants discharged in Tokyo Bay area migrate to the mountains in central Japan, i.e. the travel distance of about 150 km within one day. The distance far exceeded what was expected in simple sea breeze situation in mid-latitudes, and thus the phenomena suggested importance of combined effects of sea breeze, valley wind, and plain to plateau wind for the transport. Later Kondo (1990) numerically verified using meso-scale meteorological model that the presence of the high mountains in the central Japan, which are taller than 2000 m, is a key for the formation of the flow resulting in the medium range transport of pollutants. Kitada et al. (1998) also discussed dominant role of the high mountains of the central Japan in temporal variation of sea breezes over coastal plain area in the Pacific Ocean side, i.e. the Nohbi Plain. It was made clear more than 10 years ago, as described above, that the pollutants released from huge urban areas in the coastal Japan such as Tokyo can be transported more than 150 km within 12 hours mostly during the daytime and reach to the mountains (Kurita and Ueda, 1985). However, the synoptic scale weather with light gradient wind under high pressure system, which is preferable for the development of local winds, usually continues for several days, and the behaviors during those days of the primary and secondary pollutants, once brought in the mountainous area, are not well understood. Furthermore, recently photochemical smog episodes are frequently reported in Japan, and some people stress importance of long range transport from East Asian continent on these episodes. However, ozone observation at a mountainous site in central Japan tells primary importance of local ozone production (Kitada, et al., 2008) In this paper, to make these phenomena clear we have investigated three days behavior of the pollutants emitted in the coastal urban areas using a combined model of mesoscale meteorology (Kitada et al., 1998) and transport/chemistry/deposition of air pollutants (Kitada et al., 1993) together with airborne observation of pollutants over the Nohbi Plain and the Ise Bay area in the central Japan. The period for the investigation was 26 to 28 July, 1995.

3. NUMERICAL MODELS

a. Transport/chemistry/deposition model

The model deals with processes of advection, diffusion, chemical reactions and deposition of trace chemical species, and the basic frame of the model is described in detail in Kitada et al. (1984) , Carmichael et al. (1986) and Kitada et al. (1993). Equations are written for advected species,

$$\rho \frac{\partial C_i}{\partial t} + \rho U_j \frac{\partial C_i}{\partial x_j} = \frac{\partial}{\partial x_j}\left(\rho K_{jj} \frac{\partial C_i}{\partial x_j} \right) + R_i + S_i, \qquad i = 1, 2, \ldots, IL \tag{1}$$

where C_i denotes dimensionless concentration of species i, and R_i and S_i for chemical reaction rate and emission rate due to point source for the species i, respectively, ρ is air density, x_j spatial coordinates (i.e., j=1, 2, and3 for x, y, and z, respectively), $K_{11}(=K_{22}=K_H)$ and $K_{33}(=K_V)$ for eddy diffusivity in horizontal and vertical directions, respectively, and U_j for wind velocity in x_j direction. Meteorological fields such as wind velocity, temperature, and K_{33} were all calculated using mesoscale model described in Kitada et al. (1998). Equation (1) was applied for 44 advected species (i.e., IL=44) such as NO, NO_2, HNO_3, PAN, NH_3, NH_4NO_3, SO_2, SO_4^{2-}, O_3, H_2O_2, various anthropogenic and biogenic hydrocarbons, and others. The reaction mechanism used in the model is based on that of Lurmann et al. (1986) and α-pinene chemistry of Lloyd et al. (1983) with some revision of reaction rate coefficients from Grey et al. (1989) and DeMore et al. (1997). The model in this study consists of 159 chemical reactions. Horizontal boundary conditions for east-west, i.e.x_1, direction, for example, were expressed as follows. For inflow case,

$$-\rho K_H \frac{\partial C_i}{\partial x_1} + \rho U_j C_i = \rho U_1 C_{B,i} \tag{2}$$

where $C_{B,i}$ stands for concentration at outside of the boundary and can be renewed, and for outflow case,

$$\frac{\partial C_i}{\partial x_1} = 0 \tag{3}$$

Vertical boundary conditions were given as follows. At the earth surface boundary,

$$-\rho K_V \frac{\partial C_i}{\partial x_3} = Q_i - \rho V_{gj} C_i \tag{4}$$

where Q_i denotes the area emission source, and $V_{g,i}$ the dry deposition velocity for species i, which was evaluated by the method calculating resistances to mass transfer from air to surface (Wesely and Hicks, 1977, Sheih et al., 1979, Kitada et al., 1986 etc.). The dry deposition process was applied to the chemical species of NO_2, HNO_3, NH_3, NO_3^-, SO_2, SO_4^{2-}, O_3, PAN, and H_2O_2. At top boundary, basically the same formulations as Eqs. (2) and (3) were applied.

For 36 free radical species such as OH and HO_2, the following algebraic equations were applied by using the steady state assumption:

$$R_1 = 0, \quad i = IL+1, \cdots, IS \tag{5}$$

For Eqs. (1) through (5), terrain following coordinate transform was applied as Eq. (6):

$$\varepsilon = x_1, \quad \eta = x_2, \quad and\ \sigma = \frac{x_3 - h(x_1, x_2)}{H - h(x_1, x_2)} \tag{6}$$

where $h(x_1,x_2)$ denotes the height of topography above mean sea level(MSL) , and H is the height of top boundary above MSL and was assumed constant at 6.5 km.

b. Mesoscale meteorological model

The input meteorological fields, of flow, temperature, moisture, and eddy diffusivity, to the simulation of air pollution transport were computed with a mesoscale model with $k-\varepsilon$ turbulence module. The basis of the model is described elsewhere (Kitada et al., 1998). Here we explain only what was added into the model in this application. The model is hydrostatic, and the equations of momentum transport for horizontal directions are expressed as follows:

$$\begin{aligned}\frac{DU_i}{Dt} = &-\frac{1}{\rho}\frac{\partial p}{\partial x_{j1}} + \frac{\partial}{\partial x_k}\left(-\overline{u_j u_k}\right) + f_1\left[\delta_{j1}\left(U_2 - U_{g2}\right) - \delta_{j2}\left(U_1 - U_{g1}\right)\right] - f_2\delta_{j1}U_3 \\ &+ G_{Uj}\left(U_{obsj} - U_j\right), \qquad j = 1, 2\end{aligned} \tag{7}$$

where U_j and u_j denote the mean wind velocity to be predicted and the turbulent fluctuation, U_{gj} stands for the geostrophic wind component estimated from the observed vertical profiles of the atmospheric pressure, and U_{obsj} the observed winds, where the suffix j is for coordinate direction, i.e. x_j : j=1 for east-west, j=2 for north-south, and j=3 for vertical direction. Furthermore, p denotes the mesoscale pressure perturbation from the synoptic scale pressure field, the Coriolis parameters $f_1 = 2\Omega\cos\varphi$ and $f_2 = 2\Omega\cos\varphi$, the nudging coefficient $Gu_i = (10^{-3}\,s^{-1}$ which was selected after some numerical experiments), δ_{j1} and δ_{j2} the Kronecker's delta, and $D/Dt = \partial/\partial t + U_j\partial/\partial x_j$ the substantial derivative.

The equation of heat transport:

$$\frac{D\Theta}{Dt} = \frac{\partial}{\partial xj}\left(-\overline{u_j\theta}\right) + \frac{\Theta_0 - \Theta}{\tau_0} \tag{8}$$

where Θ, Θ_0 and θ stand for the mean potential temperature to be predicted, its synoptic scale component to be estimated using aerological data at seven observation sites in central Japan, and the turbulent fluctuation component, respectively, and τ_0 is a relaxation time scale which was set at $10^4\,s$, which was adopted after some numerical experiments. The turbulent fluxes in Eqs. (7) and (8) were evaluated using eddy diffusivity and local gradient of corresponding dependent variables, where the eddy diffusivity was calculated applying $k-\varepsilon$ turbulence model. Detail of the model is described elsewhere (Kitada et al., 1998).

4. METEOROLOGICAL INPUTS, EMISSION SOURCES AND SIMULATION CASES

a. Meteorological input data

Numerical simulations were performed for two days from 06 JST (Japan Standard Time) 26 July to 06 JST 28 July, 1995. During these days central Japan had been under the influence of high pressure system with sunny sky and light gradient wind, as seen in weather chart in Fig. 1. Thus these were typical days suitable for the development of local winds such as land and sea breeze, mountain and valley wind, and plain to/from plateau wind. Photochemical smog is also known to likely occur in this situation.

To obtain meteorological fields for the simulations of air pollution transport and chemistry, the meteorological model described above was numerically integrated in the region shown in Fig. 2a. The sizes of the region were 582.9 km × 480.5 km × 6.5 km for east-west (x), north-south (y), and vertical (z) directions, respectively. Variable grid sizes were applied with their minimum values of 2.28 km, 1.85 km, and 3 m for x, y, and z directions, respectively, and with the maximum values of 11.43 km, 9.24 km, and 200 m also for x, y, and z directions. The smallest grid size was used for the Nohbi Plain region in Fig. 2b, which is our primarily concerned area. Computed meteorological fields were for air flow, temperature, humidity, pressure, and eddy diffusivity. Observational data were taken into the computation through U_{g1}, U_{g2}, and U_{obsj} in Eq.(7), and Θ_0 in Eq.(8). These observations include: (1) aerological data at 9 sites over Japan with 12 hours interval, (2) data by 6 pilot balloons and 2 rawinsondes up to 2 km in the Nohbi Plain and Ise Bay area with one and a half hour interval during daytime, and (3) wind data at every one hour at about 360 surface meteorological observation sites operated over the whole calculation domain either by Meteorological Agency of Japan or by local governments. To construct synoptic scale pressure field, the kriging method with spherical distribution model was applied for the sparse aerological data.

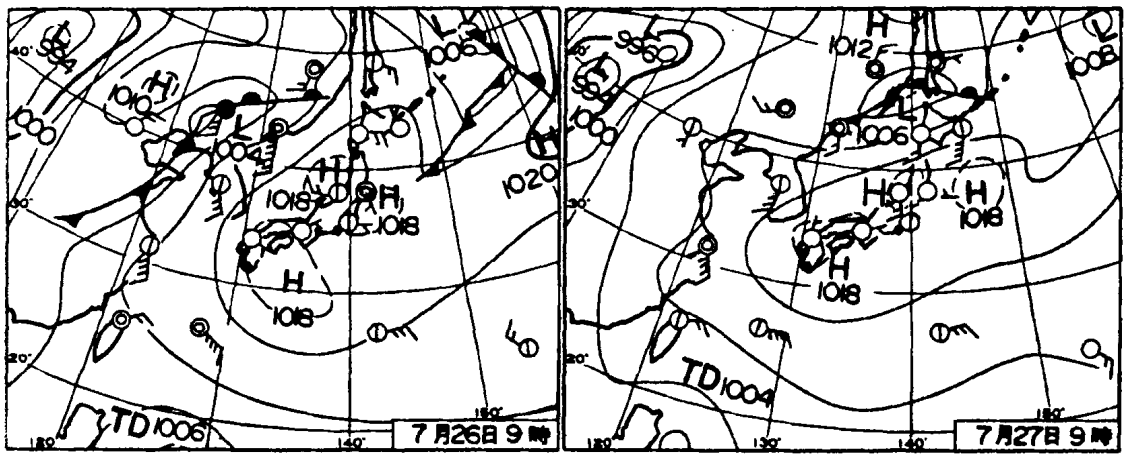

Fig. 1. Weather chart in Japan area at 09 JST (a) 26, (b) 27 July, 1995.

b. Emission sources

Emission sources of NO_x, SO_x, and various anthropogenic non-methane-hydrocarbons (hereafter abbreviated to ant-NMHC) in and near the Nohbi Plain (see calculation domain in Fig. 1b) were estimated from data compiled by the Aichi Prefectural Office (1995). NO_x and SO_x emission inventories were explicitly given with their diurnal variations in the data; they were computed on the basis of consumption of fuels in various sectors such as industries, offices, households, and traffic. The ant-NMHC were grouped into six categories of C_2H_6, C_3H_8, ALKA, C_2H_4, ALKE, and AROM as in the original chemistry model by Lurman et al.(1986). Then their emission values were evaluated as ratios of those to NO_x emission (see Table 1). Two biogenic hydrocarbons of isoprene and α-pinene were considered in the model. Emission sources of isoprene and α-pinene were estimated every one hour using the BEIS (Biogenic Emissions Inventory Systems, Pierce et al., 1990) with vegetation map compiled by Center for Natural Environment, Japan (1993). These emissions depend on solar radiation and temperature, and thus the solar radiation data were obtained at the observation sites operated both local governments and the Meteorological Agency of Japan and the temperatures were output of the meteorological model (Kitada, et al., 1998); actually the temperature at leaf skin is required, and the leaf skin temperatures were estimated by the canopy model (Okamura and Kitada, 1998).

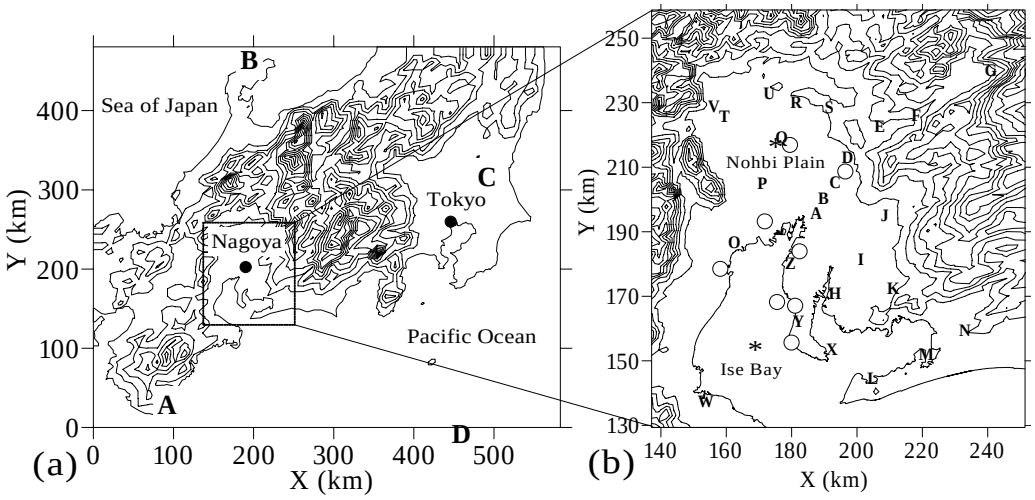

Fig. 2. Calculation domain : (a) whole area, and (b) the area magnified for the Nohbi Plain and Ise Bay. A,B,C, and D in Fig. 2a represent aerological observation sites. A through Z in Fig. 2b are for observation sites at "surface" level, open circles for pilot balloon or rawinsonde sites, and * for the locations where spiral flights were carried out, i.e. one over Ichinomiya ("Q") and another over Ise Bay.

Table 1. Summary of emission sources for the region in Fig. 1b.

Chemical species.	Emission rate (kmol day^{-1})	Ratio[3]
NO_x	7.90×10^3	1
ant－NMHC[1]	7.72×10^3	0.978
C_2H_6	0.47×10^3	(0.059)
$C_3H_8^*$	0.81×10^3	(0.103)
ALKA[#]	2.90×10^3	(0.367)
C_2H_4	0.52×10^3	(0.066)
ALKE[+]	0.70×10^3	(0.089)
AROM[=]	2.32×10^3	(0.294)
bio－NMHC[2]	2.09×10^3	
ISOP	1.6×10^3	
PINENE	0.45×10^3	

1, ant-NMHC = C_2H_6 + C_3H_8 + ALKA + C_2H_4 + ALKE + AROM.
2, bio-NMHC = ISOP + PINENE.
3, Ratio of emissions of various anthropogenic hydrocarbons to that of NO_x.
*, C_3H_8 stands for propane and benzene.
#, ALKA for $\geq C_4$ alkanes.
+, ALKE for $\geq C_3$ alkenes.
=, AROM for alkylbenzenes.

Emission sources in the whole domain (Fig. 2a) were estimated, except for the Nohbi Plain region (Fig. 2b), by using $1^\circ\times1^\circ$ Asian distribution of NO_x and SO_x (Akimoto and Narita, 1994) and $1^\circ\times1^\circ$ global distribution of isoprene (GEIA, 1998). Emissions of ant-NMHCs were computed by multiplying the NO_x emission distribution by the ratios listed in Table 1.

c. Simulation cases

Influence of emission sources of NO_x and anthropogenic and biogenic hydrocarbons on O_3 production/destruction was investigated by numerical simulations. These simulation cases are summarized in Table 2.

Case 701rx, 711rx, and 741rx do not include biogenic NMHC emission, and each of them has different strength of anthropogenic NMHC emissions while NOx emission is fixed. Case 701rxvv, 741rxvv, 751rxvv, and 711rxvv have different ant-NMHCs emission strengthwhile the same bio-NMHCs emission is included into those cases. Case 741rxnoinvv and 741rxnovv represent increased and decreased NOx emission case, respectively, with same conditions as case 741rxvv except for the NOx emission. Case 742rxvv has the same emission condition as case 741rxvv, but it turns off all the emission sources after 00 JST 27 July.

4. RESULTS AND DISCUSSION

a. Computed flow fields

Mesoscale meteorological model was integrated for four days from 00 JST 25 July to 00 JST 29 July 1995. As described above, using these outputs of the meteorological model,

Table 2. Simulation cases.

Case No.	NO_x #	ant-NMHCs #	bio-NMHCs #	Dry Deposition Velocity	Others
701rx	1	1.33	0	a	—
741rx	1	1	0	a	—
711rx	1	0.13	0	a	—
701rxvv	1	1.33	1	a	—
741rxvv (base)	1	1	1	a	—
751rxvv	1	0.67	1	a	—
711rxvv	1	0.13	1	a	—
700rxvv	1	0.0	1	a	—
741rxnoinvv	1.2	1	1	a	—
741rxnovv	0.8	1	1	a	—
741rxno6vv	0.6	1	1	a	—
761rxnovv	0.8	0.8	1	a	—
771rxnovv	0.6	0.6	1	a	—
742rxvv	1	1	1	a	off*
741rxvv2	1	1	2	a	—
741rxvv1.5	1	1	1.5	a	—
741rxvvh	1	1	0.5	a	—
741rxvvnewdepnoleaf	1	1	1	b	—
741rxvvnewdep	1	1	1	c	—

Relative emission strength to those listed in Table 1.
* All emission sources were turned off after 00 JST, i.e. midnight, on 27 July.
(a) Constant dry deposition velocities for land and water surfaces (see text for detail).
(b) Dry deposition velocities formulated using resistances of aerodynamic, surface, and residual (see text for detail).
(c) Dry deposition velocities same as in (b), but for weighted with leaf area index, LAI (see text for detail).

air pollution transport simulations were performed for two days from 06 JST 26 July to 06 JST 28 July.

Although these two days, i.e. 26 and 27 July, were typical summer days suitable for development of various local flows, there were some differences on the development of flow patterns in the Nohbi Plain. The wind fields on 26 July were more typical than those on 27 July. Usually, two types of sea breezes blow in a day in coastal area of the Nohbi Plain (see Fig. 2b); first, rather local sea breeze, the south-westerly, from Ise Bay starts to blow around noon time, and eventually, another strong sea breeze, south-easterly, from Pacific Ocean takes over the local sea breeze and continues nearly until midnight, the formation of which is strongly influenced by the Japanese Alps of the central Japan in Fig. 2a (Kitada et al., 1998). On 27 July, the sea breeze at the first stage was modified from its usual south-westerly to a westerly wind under the influence

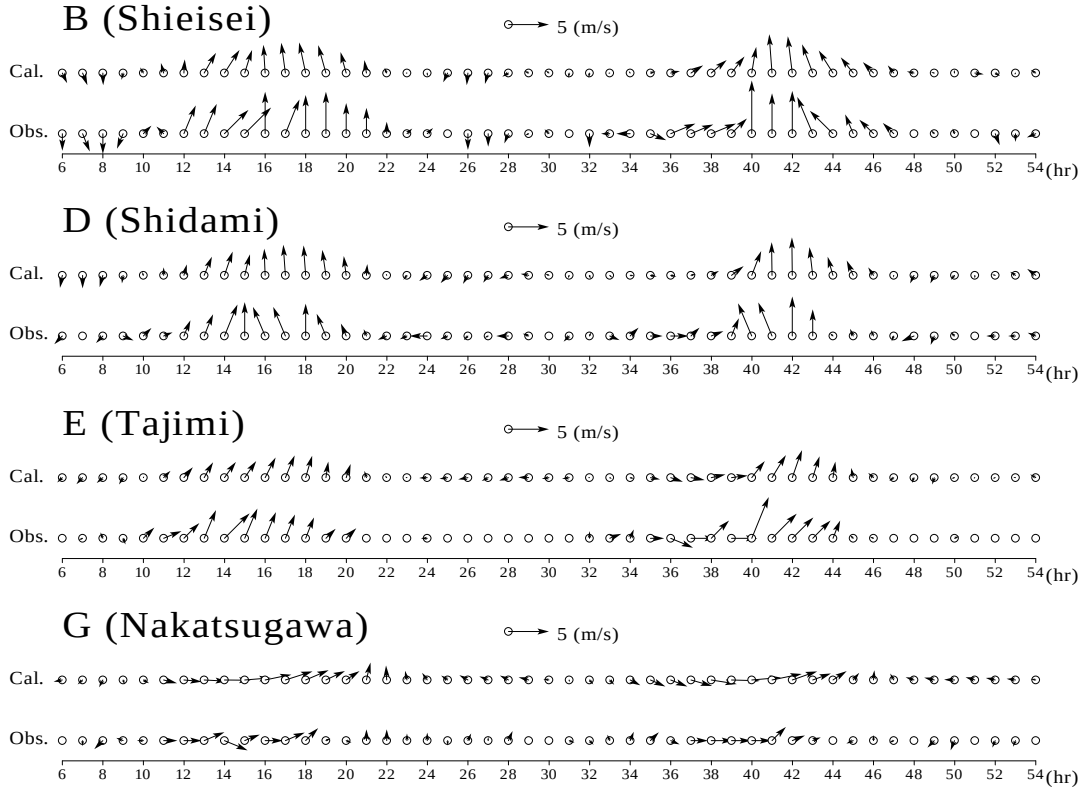

Fig. 3. Calculated vs. observed wind vectors for two days from 06 JST 26 July to 06 JST 27 July, 1995, at sitesB, D, E, and G (see Fig. 2b).

of the westerly or north-westerly winds in upper layer, and the depth of the combined sea breeze and plain-to-plateau-wind layer was suppressed and did not exceed 1 km over the Nohbi Plain in contrast to 26 July. Figure 3 shows hourly variations of both calculated and observed surface wind at 10 m above ground at the several sites, the locations of which are marked with alphabetical characters of B, D, E, and G in Fig. 2b. In Fig. 3 which compares calculated winds with those observed, the winds at B (Shieisei), and D (Shidami) from 36 to 39 hr (i.e., from 12 to 15 JST 27 July) show the "modified westerly" sea breezes compared with winds at the corresponding time on the previous day, i.e. 26 July. Figure 3 demonstrates that the calculation well simulated the observed winds.

In the simulation, winds in upper layer acquired by pilot balloon and rawinsonde were used for 4 dimensional data assimilation. Figure 4 illustrates performance of the assimilation process: Figs. 4a, 4b, and 4c show computed wind fields at 00 JST 27 July, i.e. Fig. 4a for surface wind about 10 m above the ground level(AGL) in whole calculation domain, and Fig. 4b and 4c for those at 500 m and 1000 m above mean sea level(ASL), where the observed winds are also shown with thick dotted arrow, while Figs. 4d, 4e, and 4f are the same as Fig. 4a etc. but for 15 JST 27 July. The results show appropriate modifications of the computed winds, and thus indicate that the nudging

coefficient, $G_{Uj}=10^{-3}\ s^{-1}$, the weighted average of observed winds with a weight of the reciprocal of the squared distance between grid point and observation site, and the radius of influence of 100 km below 2 km AGL all worked well. As can be seen in Fig. 4c, however, weak wind situation, i.e. no significant pressure gradient may cause some discrepancy between computed and observed winds. Due to the low wind speed, this discrepancy would not result in serious problem in transport simulation of air pollutants.

Vertical structure of wind shown in Fig. 4 also captured the characteristics found in observation on a different occasion but in the same land-sea breeze situation (Mori et al., 1998).

b. Dynamical behavior of ozone in local winds

As shown in Fig. 2b, the Nohbi Plain-Ise Bay area is bounded by mountains on the north, west, and east. This topographic feature tends to accumulate both anthropogenic and natural trace chemical species in the basin with stable stratification in the upper layer caused by the prevailing high pressure system. Reaction products produced from primary pollutants during their transport from coastal area to inland show the same behavior; ozone can be regarded as a typical species. Figure 5 plots a sequence of the north-south vertical cross sections, passing over Ichinomiya, marked with the symbol

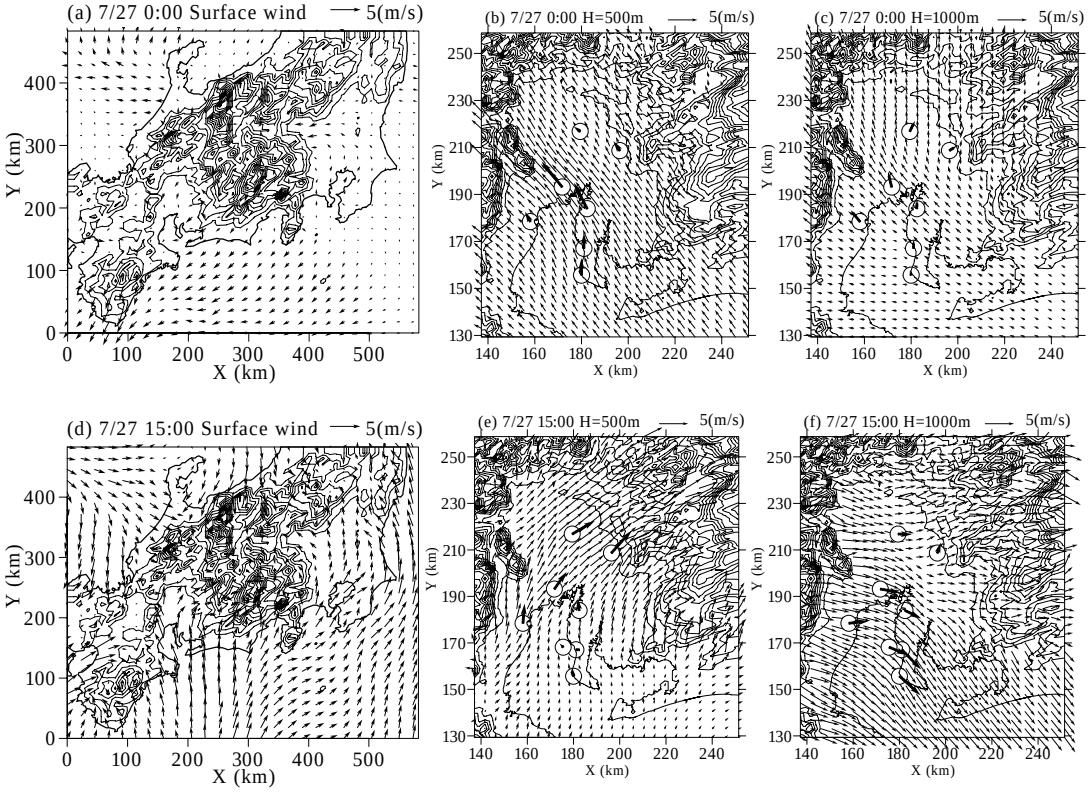

Fig. 4. Computed wind fields : (a) surface wind (at 10m above ground), (b) and (c) upper winds at 500mand 1000 m high, respectively, at 00 JST 27 July. Fig. 4 d, e, f are the same as Figs. 4 a, b,c but for 15 JST 27 July.

"Q" in Fig. 2b, of computed O_3 concentration (case 741rxvv, i.e. BASE case in Table 2)

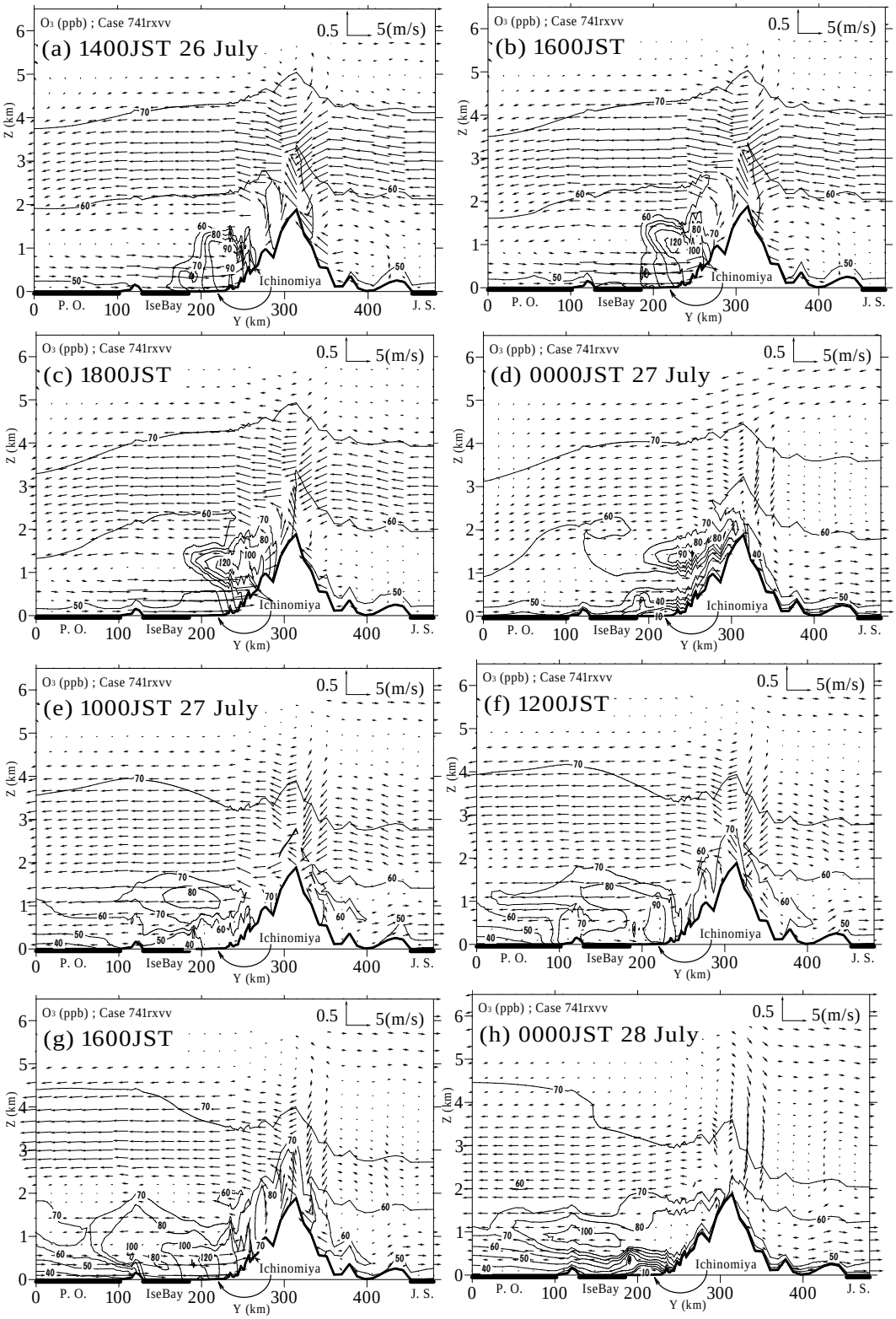

Fig. 5. Vertical cross sections of the computed O_3 (BASE; see Table 2) at x = 175 km (symbol "Q" in Fig. 2b) at (a) 14, (b) 16, (c) 18 JST on 26 July, (d) 00, (e) 10, (f) 12, (g) 16 JST 27 on July, and (h) 00 JST on 28 July.

at 14, 16, 18 JST (26 July), 00, 10, 12, 16 JST(27 July), and 00 JST(28 July), respectively. These figures illustrate the followings: (1) during the daytime O_3 concentration continues to increase near surface level in the pollutant rich air mass, originated from the coastal area and advancing inland with sea breeze and valley wind (Figs. 5a,b,c), (2) high O_3 concentration zone is formed in upper layer at around 1 km high (Fig. 5b,c) over the Nohbi Plain; the high O_3 zone is located near top of the mixed layer developed before arrival of sea breeze and in between the layers of sea breeze/valley wind and its return flow; formation of the zone is attributable to the transport of ozone and its precursors from lower level to the upper layer by both strong thermal convection before the sea breeze arrives and strong updraft when the sea breeze front passes by; these characteristics in the concentration field modified by the passage of sea breeze front agree well with the idealized 2-dimensional sea/land breeze case described in Kitada and Kitagawa (1990), (3) the high O_3 concentration zone in the upper layer at around 1.3 to 1.5km high remains during the nighttime (Fig. 5d), the layer which extends by 100km from the mountainous area to the Nohbi Plain, while O_3 concentration at the surface level is very low over the Nohbi Plain mainly due to NO_x emissions from urban area, (4) the O_3-rich air mass in the upper layer starts to move to the south over the Nohbi Plain-Ise Bay area in prevailing northerly wind in the morning on 27 July (Figs. 5e,f), while the primary pollutants-rich air mass in the lower layer over the plain area also moves to the south over Ise Bay area because of mountain wind and land breeze in the early morning; these pollutants over Ise Bay react to produce O_3 in lower layer in the morning, and (5) at noon (Fig. 5f), the developing mixed layer over the plain area entrains O_3 and probably other chemical species in the upper layer, the pollutants which were formed and emitted in the previous day; thus the background O_3 concentrations in the layer below around 1 km high over the Nohbi Plain show higher values on 27 July (Figs. 5g,h) than those on 26 July (Figs. 5b,d), demonstrating accumulation of the pollutants in the air mass extending over bay, plain, and mountain areas, when high pressure system continues for several days and a diurnal cycle of local winds is repeated.

c. Vertical profiles of O_3 —observation and calculation—

For two days of 26 and 27 July, airborne observation of O_3, NO_x etc. was carried out three times a day. In each flight, vertical profiles of the chemical species were obtained over Ise Bay and over Ichinomiya in the Nohbi Plain; the places are marked with asterisk in Fig. 2b. Figure 6a shows O_3 profiles over Ise Bay at around 09 JST 27 July; both the observed (thin solid line) and the computed (from the BASE case: square, circle, and triangle for 08, 10, and 12 JST, respectively). Observation (thin solid line) in Fig. 6a shows characteristic structure of clear double maxima at 200 m and 1200 m high. Although there is time delay, the computed O_3 profiles also show the same structure, indicating the simulation captures the characteristic behavior of O_3. Origin of the double maxima structure can be made clear by comparing case 741rxvv (BASE) with case 742rxvv (Table 2), where all the emission sources are turned off after 00 JST 27 July. The O_3 profiles in case 742rxvv (Fig. 6b) indicate that the maximum O_3 value in the lay and difference in O_3 level between the observed and the computed profile lower layer is substantially small compared with the BASE case (Fig. 6a), while the maximum in the

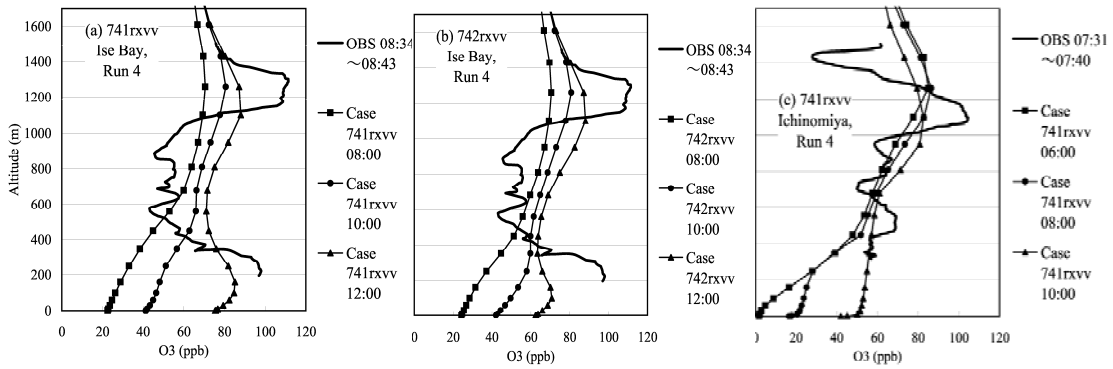

Fig. 6. Vertical profiles of O_3 observed and calculated over (a) and (b) Ise Bay and (c) Ichinomiya. The location of Ichinomiya is marked with "Q" and "*****" in Fig. 2b. The observations were carried out from 0730 to 0900 JST 27 July.

upper layer at 1200 m is almost same as in Fig. 6a. This suggests that the maximum in the upper layer consisted of the O_3 produced on the previous day over the Nohbi Plain and mountainous area and transported back by the northerly or northwesterly wind blowing at the 1200 m level in the morning, while the another maximum in the lower layer was mainly caused by the photochemical production from the fresh precursors discharged in the rim area of Ise Bay and carried over Ise Bay by northerly and/or westerly land breeze in the morning of 27 July.

Figure 6c is the same as Fig.6a but for Ichinomiya (Fig. 2b) in the Nohbi Plain at around 08 JST. The computed O_3 profiles (Fig. 6c) also reasonably well simulate the observation. The calculated profiles at 06 and 08 JST show low concentrations near

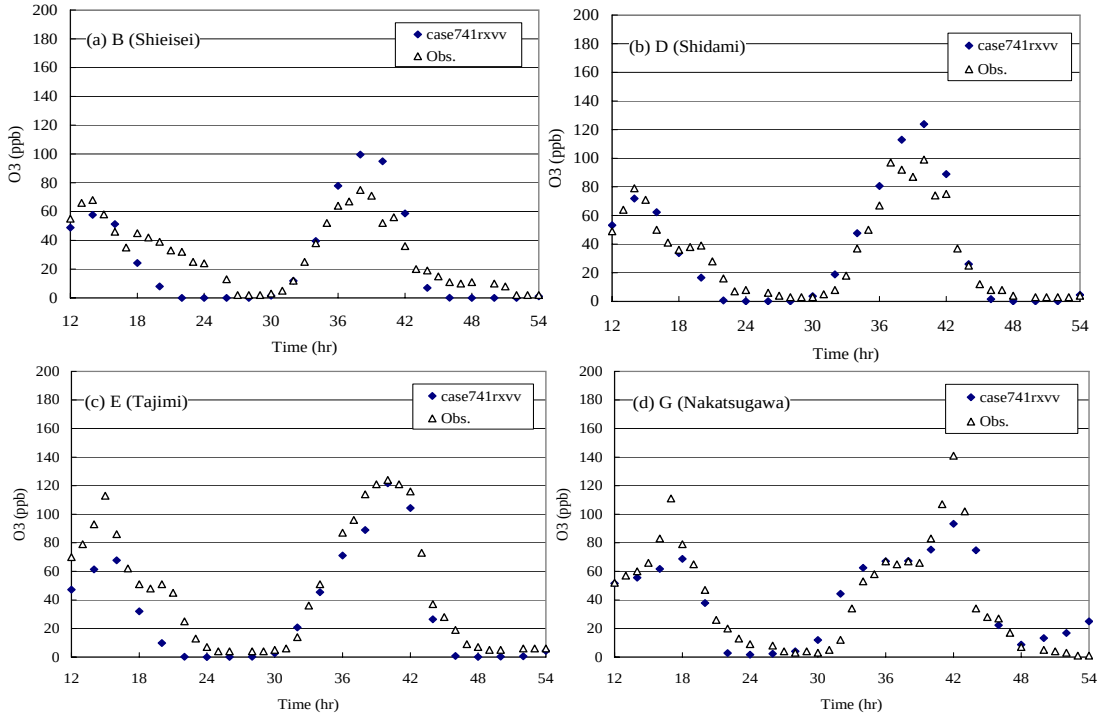

Fig. 7. Comparison between observed and calculated O_3 concentrations at sites B, D, G, and E (case 741rxvv, i.e. BASE). The "12 hr" means 12 JST on 26 July

ground level because NO_x sources are strong and the scavenging of O_3 is faster than its photochemical production during the time.

d. Tracking of O_3 transport along a major river

Local winds tend to develop along river and valley. Thus transport of air pollution also likely occurs along the river. Figure 7 shows temporal variations of both observed and computed O_3 (BASE in Table 2) at the sites of B, D, E, and G (Fig. 2b), which are located along the Shonai River and the Kiso River.

On the 2nd day (27 July) starting from 24 hr in Fig. 7, the observed maximum O_3 concentrations at these sites show clear time delay with the earliest maximum occurring at 14 JST at site "B" near the coast and the latest maximum being at 18 JST at the most inland site "G" (Fig. 2b). This time delay and the sharp peak concentration in the late afternoon at site "G" demonstrate the ozone came along the rivers with polluted air mass from the coastal area. Figure 7 also shows the "BASE" case well simulates these characteristic O_3 pattern at each site.

Temporal variation of the vertical O_3 profile (BASE) at site "G" (Fig. 8) suggests that the O_3 - rich air mass first arrived at the site at 18 JST, then the polluted air mass continued to fill space in the valley until mountain wind and plateau-to-plain wind started to blow around 02 - 04 JST (Figs. 8b, c); the high O_3 air filled the valley up to the ridge height surrounding site G, i.e. around 1200 m in altitude, as indicated with arrow in Fig. 8, and (3) the surface O_3 concentration peaked at 18 JST and decreased

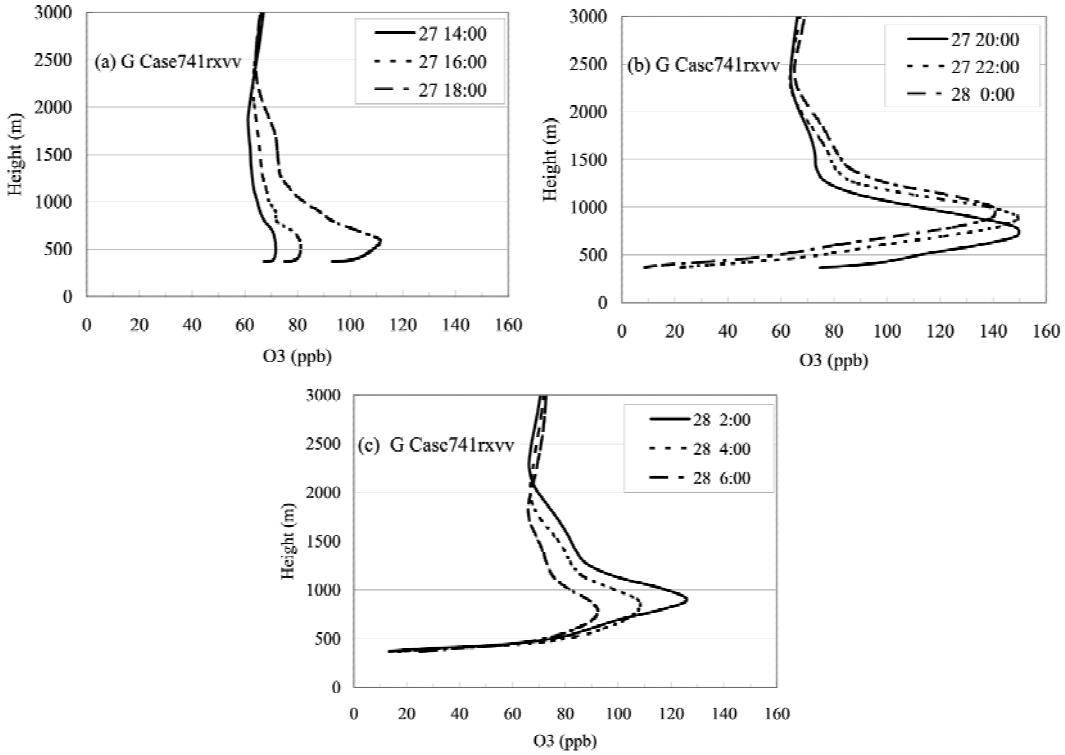

Fig. 8. Computed vertical profile of O_3 at site "G" (BASE case). (a) 14, 16, and 18 JST 27 July, (b) 20, 22 JST 27 July, and 00 JST 28 July, and (c) 2, 4, and 6 JST 28 July. Arrows show the height of ridge surrounding the valley in which site "G" locates.

after that due to destruction within stably stratified surface layer formed by radiational cooling.

e. Effect of biogenic hydrocarbons on O_3 concentration

Quantitative understanding of the effect of biogenic hydrocarbons on O_3 production etc. is important for better prediction of performance of designed emission control on anthropogenic sources. The effect was evaluated by examining cases with and without the natural source (see Table 2).

The “BASE" emission source distributions of isoprene and α-pinene were estimated

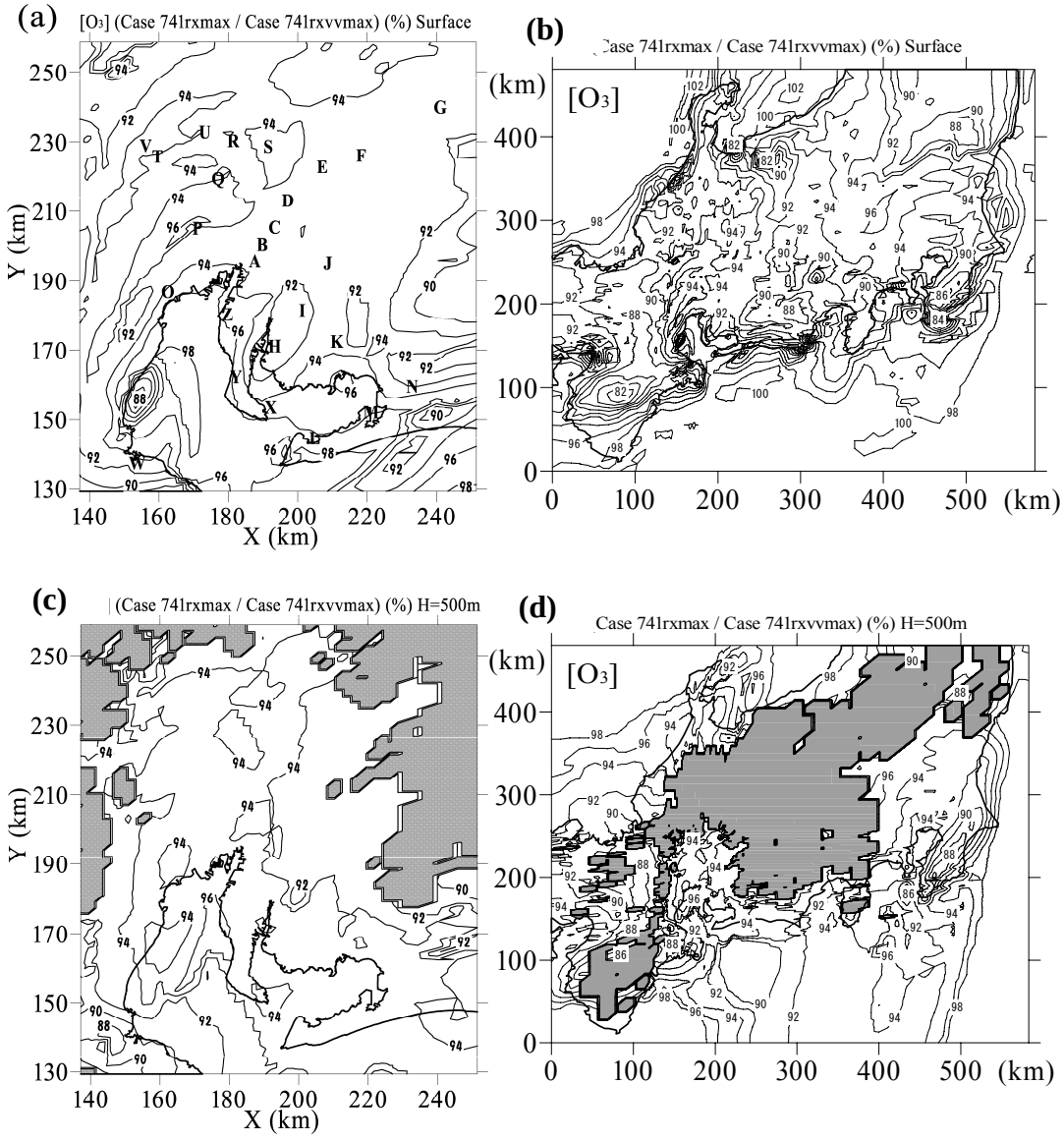

Fig. 10. Horizontal distribution of the ratio of max O_3 in case 741rx to that in BASE (case 741rxvv) on 27 July, 1995: (a) surface level, and (c) 500 m AMSL, and (e) 1200 m ASL in the Nohbi Plain-Ise Bay area, and (b), and (d) are the same but for the central Japan.

using BEIS and a map of vegetation type, as described in the previous subsection (see Table 1). Because of its nature isoprene is emitted only during the daytime, while α-pinene is discharged also during the nighttime.

Figure 9 compares O_3 in the BASE case (case 741rxvv, dashed line) with that in case 741rx (solid line), i.e. without biogenic emissions. Increase of maximum O_3 concentration due to bio-NMHC emissions on the 2nd day, i.e. 27 July, is about 10 ppb at all sites of B, D, E, and G (see Fig. 2b), and thus does not show significant difference among the sites which are aligned along one of the major directions of mass transport in the Nohbi Plain.

Figure 10 illustrates horizontal distribution of the percentage of maximum O_3 in case 741rx (no bio-NMHC sources) to that in case 741rxvv (BASE; with bio-NMHCs sources) at the surface level (Figs. 10a, b), and at the height of 500m AMSL (Figs. 10c, d) on 27 July 1995, showing spatial variation of relative importance of biogenic hydrocarbons on O_3 production; 100% minus contour value in Fig. 10 indicates contribution of bio-NMHC to the maximum O_3 concentration in percentage.

In the Nohbi Plain (Fig. 10a) relatively uniform and small contribution, to the maximum ozone, of bio-NMHC between 6% (=100-94) to 8% (100-92) is predicted, and this means that both NOx and ant-NMHCs are supplied from the coastal emission area enough to produce O_3, and neither an excess-NOx condition nor shortage-of-NMHCs situation does occur during the daytime transport. A similar observation is also possible in the Kanto Plain, Tokyo area at around x=450 km and y=300 km in Fig. 10b. On the other hand, an interesting contrast can be seen in near Osaka area at x=50km and y=150km in Fig. 10b; that is, Fig. 10b shows the maximum ozone concentration in Osaka could be reduced by more than 10 % without biogenic NMHCs emission, and the area widely spreads over the down-sea-breeze region of the anthropogenic emissions in the Osaka Plain, where the sea breeze blows from west to east. The Osaka Plain is smaller than the Kanto and the Nohbi Plains, i.e. distance from coast to mountainous area is much shorter. Thus the polluted air mass from the Osaka Plain reaches the mountains (the Kii Peninsula) in the early afternoon, and biogenic NMHCs in the mountains could more effectively contribute to the ozone production.

Generally speaking, effect of biogenic NMHCs on O_3 production is large when the air mass from urban area is mixed with the biogenic NMHCs earlier in the daytime, and, of course, higher the concentrations of the biogenic NMHCs are, larger their effects on ozone production are. High contributions in the Bohsoh Peninsula at x=450 km and y=200km may be due to pre-loading of bio-NMHCs over coastal mountains into the sea breeze before the breeze passing over anthropogenic emission area. Another high zone at x=250km and y=180km is also due to the pre-loading from high bio-NMHCs emissions in this area where ant-NMHCs emissions are relatively weak. Figure 10b also shows, in most of the central mountainous area, bio-NMHCs contribute to daily maximum O_3 concentration by 6 - 8 %.

The patterns at 500m AMSL (Figs. 10c,d) are almost similar to those at the surface; it is suggested that high contribution of the bio-NMHCs at x=250km over the coast of Pacific Ocean (Fig. 10b) propagated toward the Pacific Ocean (Fig. 10d) due to the effect of synoptic scale flow on the day, blowing southward to south-westward in upper layer.

The bio-NMHCs emitted in mountainous area have to be mixed with the anthropogenic NOx discharged over the coastal urban areas so as to produce O_3, and

such a contact of those chemical species at this height is only possible at high mountains relatively close to coastal urban area.

Figures 11a,b,c show the maximum ozone concentration on 27 July in BASE case: (a) surface, (b) 500m ASL, and (c) 1200m ASL. We did not compare the calculated ozone concentration with the observed in the Knato Plain (Tokyo area) and the Osaka Plain since in these areas the anthropogenic emission sources evaluated from $1^{\circ} \times 1^{\circ}$

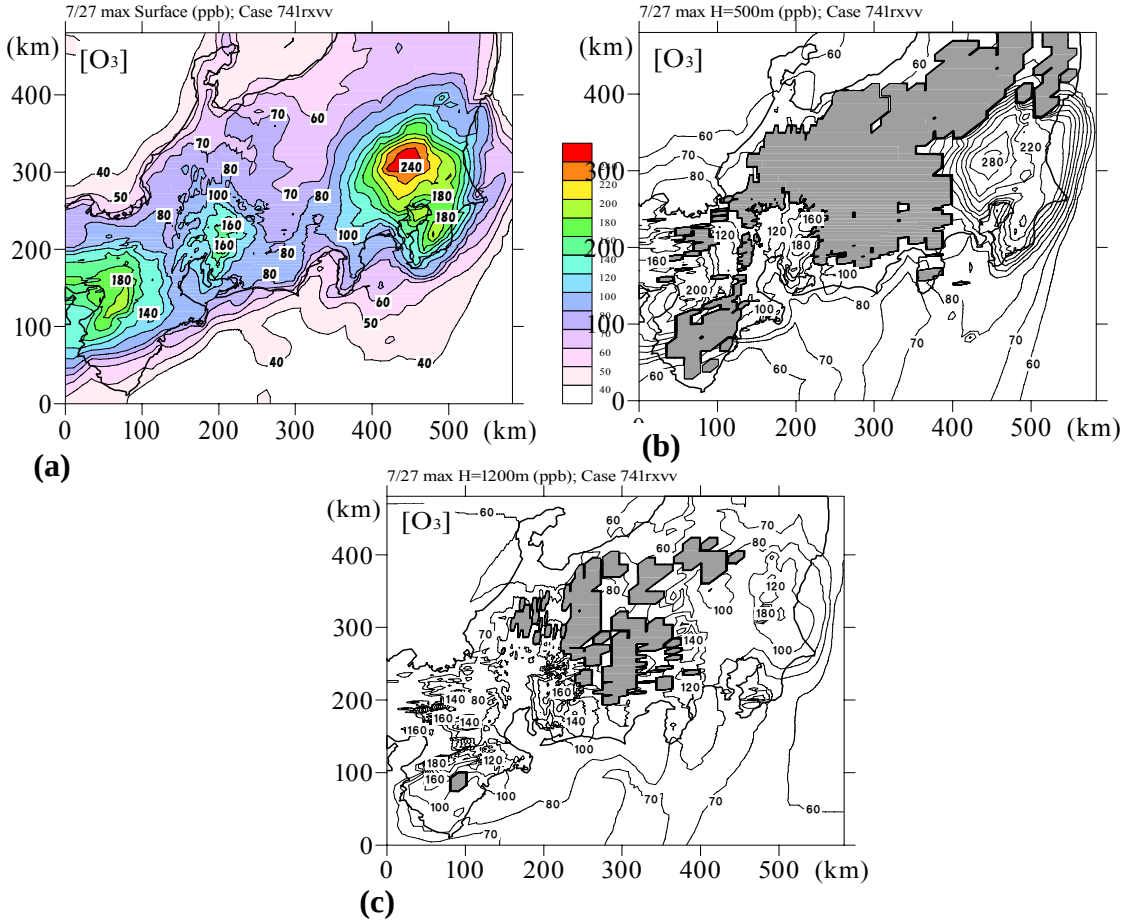

Fig. 11. Distributions of calculated $(O_3)_{max}$ on 27 July at (a) surface, (b) 500m ASL, and (c) 100m ASL in BASE case

global distribution (Akimoto and Narita, 1994) are used and they do not give fine resolution. However from these figures some observations may be possible: first, high O_3 concentration air over 100ppb widely extends in the main coastal urban areas of the Pacific Ocean side, maximum ozone concentration exceeding 100ppb over most of the plains; secondly, the ozone concentrations over plain areas show their maximum values at the middle of mixing layer, as many previous researches point out; thirdly, Fig. 11c suggests that at 1200m ASL the highest ozone concentrations appear over mountainous areas in the Kii Peninsula, east and north of the Nohbi Plain, and west and north of the Kanto Plain.

f. Sensitivity of O_3 concentration to anthropogenic emission sources of NMHCs and NOx

Sensitivity of the maximum O_3 concentration to ant-NMHCs and NOx emission in the Nohbi Plain was investigated using results of cases 701rxvv, 741rxvv, 751rxw, and 711rxvv in Table 2.

Figure 12 plots computed maximum O_3 concentration (on 27 July) at sites B, D, E, and G (Fig. 1b) to ant-NMHCs emissions. These Figs. 12a, b, c show more or less that the maximum O_3 concentration at each site is sensitive to anthropogenic NMHCs emission. For example, at site B in Nagoya a 20% reduction of ant-NMHCs emissions resulted in by 15 ppb cut of the maximum O_3 concentration; similarly, by 14 and 13 ppb at site D and E, respectively. In contrast, at the mountain site G, only small decrease in its maximum O_3, i.e. 2 ppb, was predicted. These again suggest that ant-NMHCs emissions limit O_3 production in the Nohbi Plain, but not in the mountainous area.

Open circle in Fig. 12 shows case 741rxvvh (Table 2); i.e., biogenic NMHCs emissions were cut by 50 % from the BASE case, and it suggests only negligible reduction in max O_3 can occur with halved bio-NMHC emissions.

Both of the comparison of O_3 between cases with and without bio-NMHCs in Fig. 9 and the result in Fig 12 showing almost no change of max O_3 demonstrate highly non-linear nature of the role of bio-NMHC in O_3 chemistry (McKeen et al., 1991, Roselle et al., 1991 etc.). This suggests that (1) at sites B, D, and E, which are located in either central or northeastern part of the Nohbi Plain, NO_x was sufficiently fed for

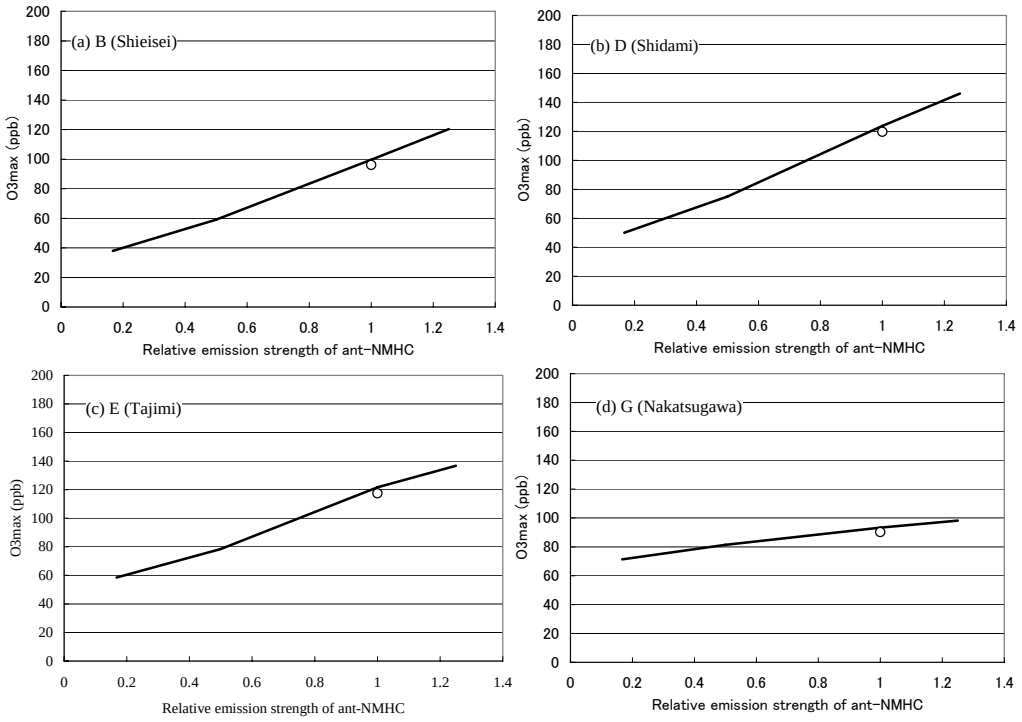

Fig. 12 Sensitivity of maximum O_3 (27 July) to anthropogenic NMHCs emission ; results of cases 701rxvv, 741rxvv, 751rxvv, and 711rxvv are used. ant-NMHCs emission is normalized by that in case 741rxvv. Open circle denotes the case 741rxvvh.

photochemical O_3 production, but ant-NMHC were not, i.e. hydrocarbon-limiting situation, and (2) the site G is in mountainous region (Fig. 2b), amount of ant-NMHC was adequate compared with NO_x, i.e NO_x-limiting situation.

Figure 13 illustrates sensitivity of O_3 concentration at the sites of B, D, E, and G (Fig.

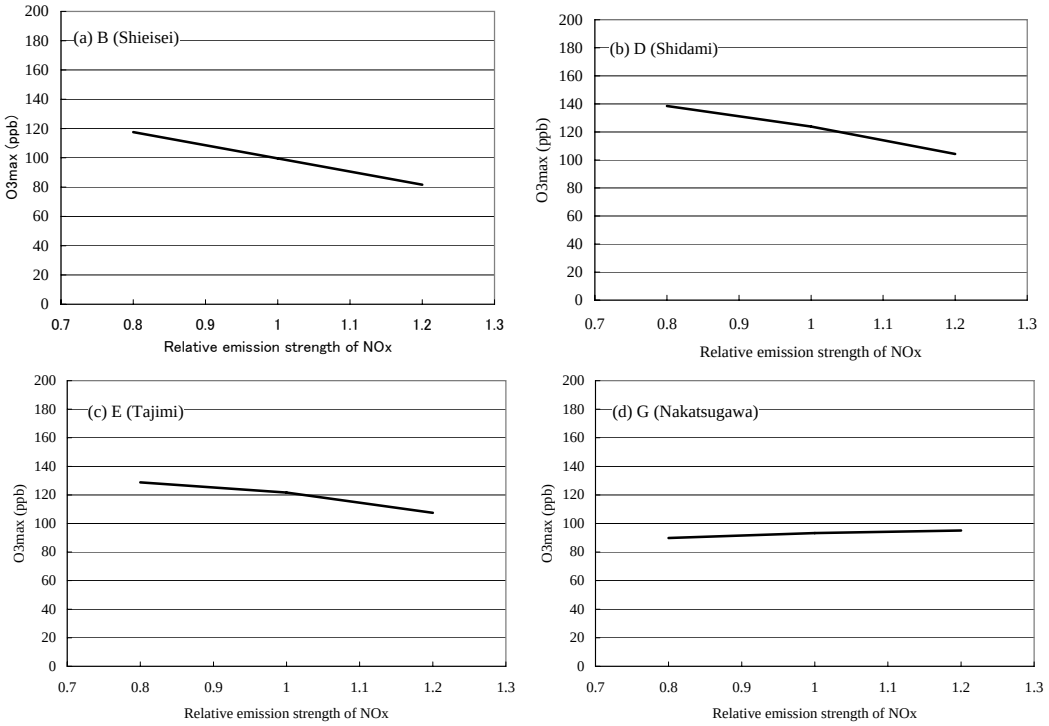

Fig. 13. Sensitivity of maximum O_3 concentration, on 27 July, to NO_x emission : the results of cases 741rxvv, 741rxnoinvv, and 741rxnovv (Table 2) are used. NO_x emission is normalized by that in case 741rxvv (BASE).

2b) to NOx emission in the calculation domain. Figures 13a,b,c suggest ozone production at the sites of B, D, and E in the urban area is in the excess-of-NOx condition; thus decrease in NOx emission is leading to increase in O_3 concentration. In contrast to these urban sites, ozone at the site G in mountainous rural area (see Fig. 2b) shows a slight increase with increased NOx emission, indicating ozone production in the area of "G" is rather in the excess-of-hydrocarbon condition. Abundant biogenic hydrocarbons in the mountain area explain this situation. In summary, the urban area including Nagoya as a central mega-city in the Nohbi Plain is in the excess-of-NOx situation, and extent of the "excess" gradually decreases in the suburbs. Finally in rural mountainous area, the situation changes to the excess-of-hydrocarbon condition.

g Calculated high concentrations of photochemical reaction products in mountainous area during nighttime

As can be expected from the topography in the domain (Fig. 2a), local flows such as sea breeze, valley wind, and plain-to-plateau wind tend to converge to the central mountainous area during daytime. Thus various photochemical products may form high concentration zone at high altitudes, e.g. Fig. 5d.

Figure 14 shows (a) O_3, (b) SO_4^{2-}, and (c) $HNO_3 + NO_3^-$ concentrations at 1500 m high on 00 JST 27 July (BASE case). Two high concentration zones can be seen; one is Chichibu, Tanzawa, and Izu area to the west of Tokyo. The other is Hida and Takayama area to the north of Nagoya. These pollutants are products of photochemical smog reactions and are originated from the huge urban areas of Tokyo and Nagoya. Mountains in Chichibu and Tanzawa have already suffered the damage to vegetation by acidic fog (Igawa et al., 1998).

In Hida area to the north of Nagoya, such an effect on the vegetation has not yet been clarified. However, Fig. 5 strongly suggests the same damage as Chichibu and Tanzawa may be taking place also in the Hida area. Statistical study on the local flows in central Japan indicates that the meteorological condition leading to the pollutants' transport

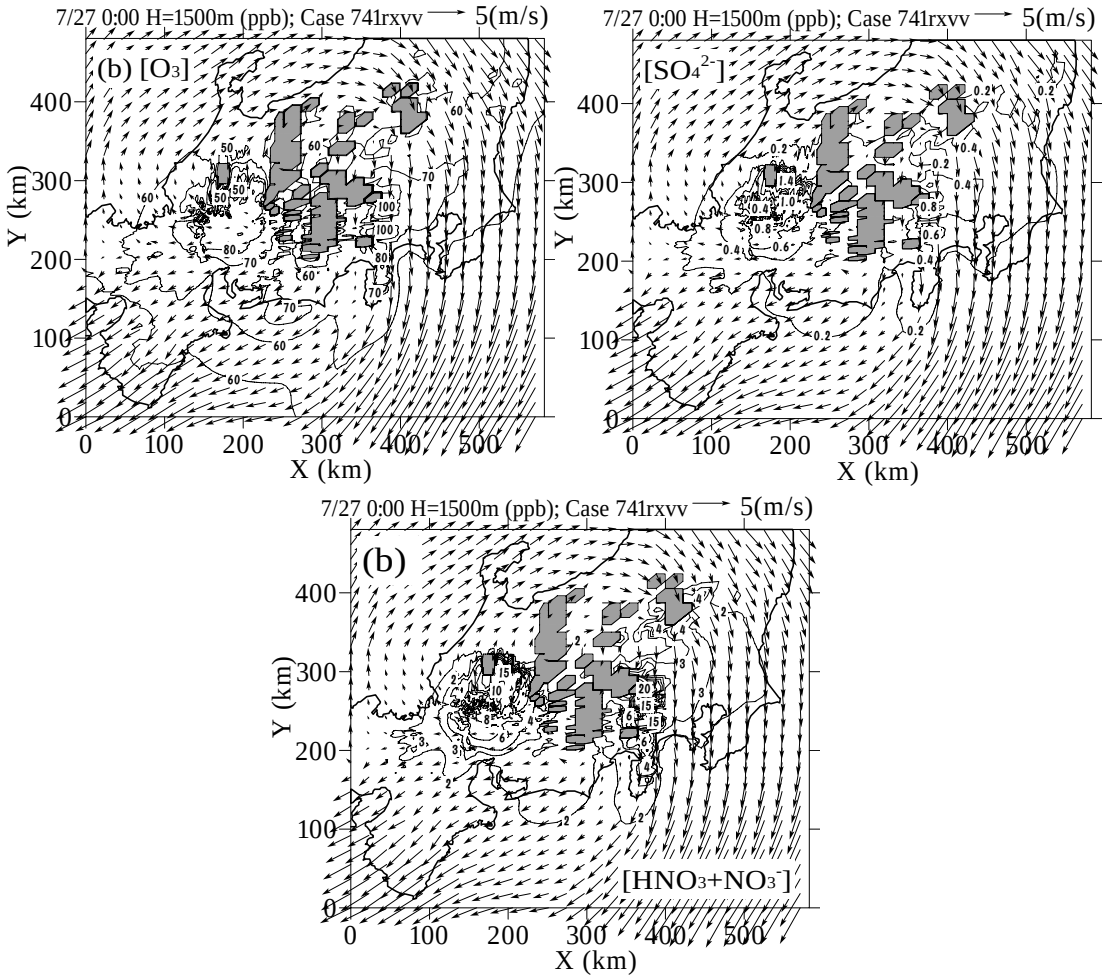

Fig. 14. Computed horizontal cross sections of (a) O_3, (b) SO_4^{2-}, (c) $HNO_3 + NO_3^-$ at 1500 m high on 00 JST 27 July (case 741rxvv, i.e. BASE).

found in Figs. 5 and 14 occurs quite frequently such as for about 80 days during warm season from April to October (Mori et al., 1994).

Figure 15 also shows (a) O_3, (b) SO_4^{2-}, (c) $HNO_3 + NO_3^-$ concentrations for case 741rx, i.e. without biogenic hydrocarbons. Comparison between Figs. 14 and 15 demonstrates effects of biogenic hydrocarbons on photochemical products in remote

area : (1) O_3 production can be enhanced by the biogenic hydrocarbons and the concentrations are increased by 20 ppb in Chichibu, Tanzawa, and Izu areas near Tokyo,

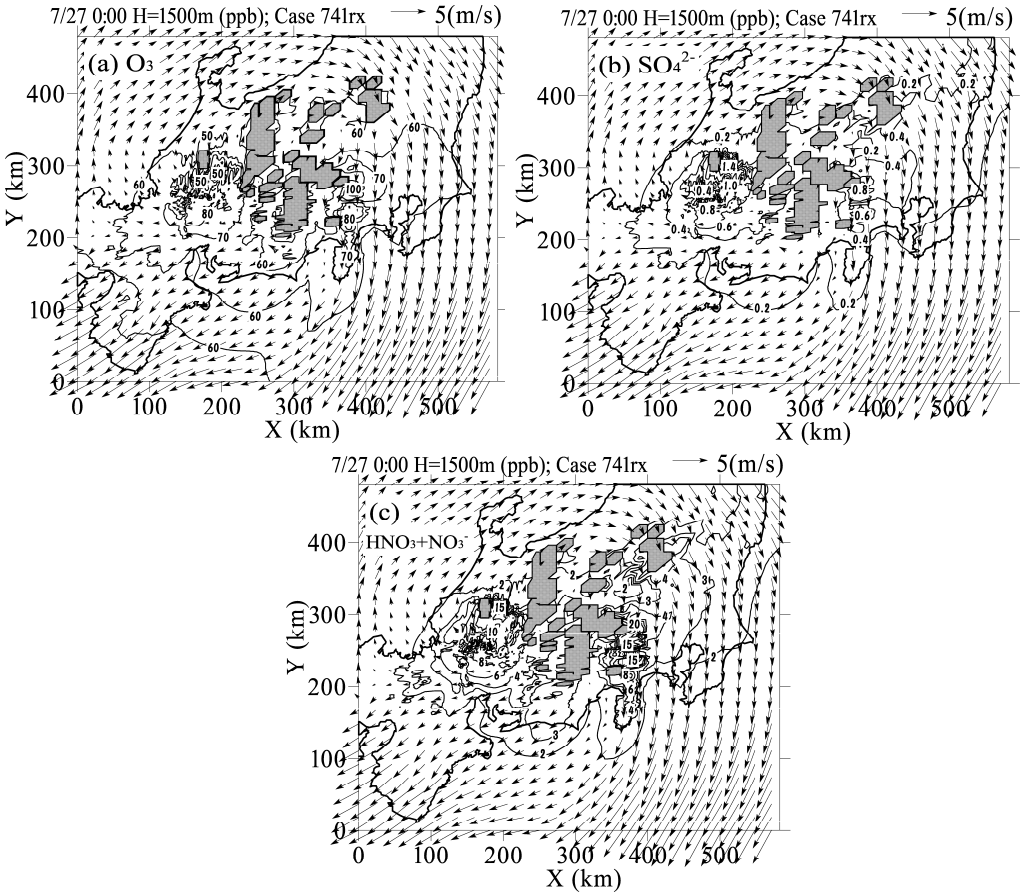

Fig. 15. Same as Fig. 14 but for case 741rx, i.e. without biogenic hydrocarbons.

and by 10 ppb in Hida and Takayama areas near Nagoya ; (2) sulfate concentrations are also increased by about 0.2 ppb; and (3) nitric acid and nitrate are drastically decreased by 5 - 10 ppb, and these lost nitric acid and nitrate are turned to biogenic nitrate.

5. SUMMARY AND CONCLUSIONS

To see the multiple days' behavior of air pollutants released in coastal urban areas in Japan, two days numerical simulations of meso-scale flow and air pollution transport were performed from 06 JST 26 July to 06 JST 28 July 1995 for central Japan. High pressure system, with light gradient wind and sunny sky, was dominant over the region. Thus various types of local flows developed during the simulated time. Furthermore, in the Nohbi Plain 3 dimensional observations using aircraft, pilot balloon; and rawinsonde were performed for the same time. These observed data were utilized in simulations as inputs for nudging computed wind, and for evaluation of computed concentration profiles.

Analysis was focused on (1) clarifying two days' behavior O_3 in developed local wind system. (2) tracking polluted air mass along a river-valley topography. (3)

quantifying effects of biogenic NMHCs on O_3, SO_4^{2-}, and nitrate productions. (4) sensitivity of maximum O_3 concentration to emissions of ant-NMHCs and NO_x.

Part of the obtained results is as follows : (1) Pollutants released in coastal urban area are transported, with being chemically transformed, to mountainous area by midnight, and forms high concentration zone of O_3, SO_4^{2-}, HNO_3 etc. at around 1500 m in altitude. Then, on the following day these pollutants are backed to the upper layer over the coastal area. (2) In summer season over the Nohbi Plain, air mass may be in (non-methane-) hydrocarbon limiting situation on O_3 production, and maximum O_3 concentration was quite insensitive to increase/decrease of NO_x emission by 20 %. (3) Inclusion of biogenic hydrocarbon emission into simulation very much enhanced O_3 and SO_4^{2-} concentrations on mountainside at 1500 m high, but decreased HNO_3 and NO_3^- by providing NO_x pathway to biogenic nitrate.

ACKNOWLEDGMENT

This work was supported in part by the Ministry of Education, Culture, and Science, Japan through Grant-in-Aid for Scientific Research (B), No. 17360256 and Global Environment Research Fund, No. C-051 by Ministry of the Environment, Japan.

REFERENCES

Aichi Prefectural Office, Japan, 1995, Data compiled by Division for Environment.

Akimoto, H., and Narita, H., 1994, Distribution of SO_2, NO_x and CO_2 emissions from fuel combustion and industrial activities in Asia with $1^\circ \times 1^\circ$ resolution. *Atmos. Environ.*, 28:213.

GEIA, 1998, Emission source distribution of biogenic hydrocarbons. Web site http://blueskies.sprl.umich.edu/geia/

Gery, M. W., Whitten, G. Z., Killus, J. P., and Dodge, M. C., 1989, A photochemical kinetics mechanism for urban and regional scale computer modeling. *J. Geophys. Res.*, 94:12925.

Guenther, A., Hewitt, C. N., Erickson, D., Fall, R., Geron, C., Graedel, T., Harley, P., Klinger, L., McKay, W. A., Pierce, T., Scholes, B., Steinbrecher, R., Tallamraju, R., Taylor, J., and Zimmerman, P., 1995, A global model of natural volatile organic compound emissions. *J. Geophys. Res.*, 100:8873.

Igawa, M., Tsutsumi, Y., Mori, T., and Okochi, H., 1998, Fogwater chemistry at a mountainside forest and the estimation of the air pollutant deposition via fog droplets based on th atmospheric quality at the mountain base. *Environ. Sci. Technol.*, 32:1566.

Kitada, T., Carmichael, G.R. and Peters, L.K., 1986, Effects of dry deposition on the concentration-distributions of atmospheric pollutants within land- and sea-breeze circulations. *Atmos. Environ.*, 20:10, 1999-2010.

Kitada, T., Lee, P.C.-S., and Ueda, H., 1993, Numerical modeling of long-range transport of acidic species in association with meso-β-convective clouds across the Japan sea resulting in acid snow over coastal Japan -I. Model description and qualitative verifications. *Atmos. Environ.*, 27A:1061.

Kitada, T. Nagano, M., and Arai, K., 2008, Ozone in mountainous central Japan on the Pacific Ocean side: seasonal variation and characteristic meso-scale transport, *Proc. 15th Seminar of JSPS-MOE Core University Program on Urban Environment, 157-165.*

Kitada, T., Okamura, K., Nakanishi, H., and Mori, H., 2000, Production and transport of ozone in local flows over central Japan –comparison of numerical calculation with airborne observation-. *Air Pollution Modeling and Its Application XIII*, Kluwer Academic/Plenum Pub. Co., 95-105.

Kitada, T., Okamura, K., and Tanaka, S., 1998, Effects of topography and urbanization on local winds and thermal environment in Nohbi Plain, coastal region of central Japan -A numerical analysis by meso-scale meteorological model with k-ε turbulence model. *J. Appl. Meteor.*, 37:1026-1046.

Kurita, H., Sasaki, K., Muroga, H., Ueda, H., and Wakamatsu, S., 1985, Long-range transport of air pollution under light gradient wind conditions. *J. Climate Appl. Meteorol.*, 24:133.

Lloyd, A.C., Atkinson, R., Lurmann, F.W., and Nitta, B., 1983, Modeling potential ozone impacts from natural hydrocarbons - I. Development and testing of a chemical mechanism for the NO_x-air photooxidations of isoprene and α-pinene under ambient conditions. *Atmos. Environ.*, 17:1931-1950.

Lurmann, F.W., Lloyd, A.C., and Atkinson, R., 1986, A chemical mechanism for use in long-range transport/acid deposition computer modeling. *J. Geophys. Res.*, 91:10905.

McKeen, S. A., Hsie, E. -Y., and Liu, S. C., 1991, A study of the dependence of rural ozone on ozone precursors in the Eastern United States. *J. Geophys. Res.*, 96:15,337.

Mori, H., Kitada, T., and Iyoda, K., 1998, Vertical structure of land and sea breezes in the Nohbi plain during a passage of an anticyclone over the central Japan. *Tenki*, Meteorol. Soc. Japan, 45:515 (in Japanese).

Mori, H., Ogawa, H., and Kitada, T., 1994, Characteristics of land and sea breezes in the Nobi plain, and the conditions of occurrence of the "extended sea breeze". *Tenki*, Meteorol. Soc. Japan, 41:379 (in Japanese).

Nakanishi, H., 1996, Emission sources and concentrations of non-methane hydrocarbons over the Nohbi plain in central Japan. *Toyohashi Univ. Technology, B.S. thesis*, 42 (in Japanese).

NASA Panel for Data Evaluation, 1997, Chemical Kinetics and Photochemical Data for Use in Stratospheric Modeling, Evaluation No. 12, NASA JPL.

Shawn, J. R., Thomas, E. P., and Kenneth, L. S., 1991, The sensitivity of regional ozone modeling to biogenic hydrocarbons. *J. Geophys. Res.*, 96:7371.

Sheih, C.M., Wesely, M.L., and Hicks, B.B., 1979, Estimated dry deposition velocities of sulfur over the eastern United States and surrounding regions. *Atmos. Environ.*, 12, 2055-2087.

Slinn, W.G.N., 1977, Some approximations for the wet and dry removal of particles and gases from the atmosphere. *Water, Air, and Soil Poll.*, 7:513.

Wesely, M.L., and Hicks, B.B., 1977, Some factors that affect the deposition rates of sulfur dioxide and similar gases on vegetation. *J. Geophys. Res.*, 100:11,447.

Yokouchi, Y., 1994, Seasonal and diurnal variation of isoprene and its reaction products in a semi-rural area. *Atmos. Environ.*, 28:2651.